Preparation and characterization of the semiconductor CuMnO2 by sol-gel route

Nadia Benreguia, Antoine Barnabé, Mohamed Trari

Preparation and characterization of the semiconductor $CuMnO_2$ by sol-gel route

N. Benreguia [a], A. Barnabé [b], M. Trari [a,*]

[a] Laboratory of Storage and Valorization of Renewable Energies, Faculty of Chemistry (USTHB), BP 32, Algiers, 16111 Algeria
[b] Centre Inter-Universitaire de Recherche et d'Ingénierie des Matériaux (CIRIMAT)-UMR CNRS 5085, Toulouse III, 118 Route de Narbonne, Toulouse Cedex 09, 31062 France

ARTICLE INFO

Keywords:
Crednerite $CuMnO_2$
Sol–gel method
Scanning electron microscopy
Raman spectrum
Optical property

ABSTRACT

Nano crystallites of the crednerite $CuMnO_2$ are prepared by sol gel method with two step annealing process. The powder heated at 450 °C under air flow shows a mixture of CuO, Mn_2O_3 and $Cu_xMn_{3-x}O_4$. However, when calcined at 900 °C under N_2 atmosphere, the crednerite $CuMnO_2$ with a monoclinic structure (space group: $C2/m$) is obtained. The Raman spectrum shows a single peak at 679 cm^{-1} as signed to A_{1g} mode whereas the infrared analysis confirms the linearity of CuO_2^{3-} units. The optical transition at 1.70 eV, determined from the diffuse reflectance is attributed to the inter band d d transi tion of Cu^{+} ion. The oxide exhibits semiconducting properties with an activation energy of 0.21 eV. The photo electrochemical measurement shows p type conduction due to O^{2-} insertion in the two dimen sional lattice. The flat band potential (+0.12 V_{SCE}), indicates a cationic character of both valence and conduction bands deriving from Cu^{+}: $3d$ orbital.

1. Introduction

The $3d$ metals based oxides A Mn O (A=La, Ag, Cu….) possess interesting physical properties because of the presence of the Jahn Teller (J T) ion Mn^{3+}[1 4]. Among the candidates, $CuMnO_2$ has two different structures depending on the temperature of the heat treatment: namely the hexagonal variety at high temperature [5] and the monoclinic form crednerite at room temperature [6]. The crednerite $CuMnO_2$ involves magnetic Mn_2O_3 sheets and ex citonic Cu_2O semiconducting layers and can be applied as hydro gen catalyst under illumination owing to the high energy of the conduction band [7]. It has also been used for the removal of toxic gases like carbon monoxide and nitrous oxides [8].

The synthesis by sol gel route permitted the formation of many oxides in various configurations (monolithic, thin films, fibers, powders). This great diversity is attractive in various technological fields like optic, electronic, biomaterials, photocatalysis etc…. In the sol gel method, the oxides are treated at temperatures lower than those of conventional synthetic routes and offer the ability to com bine organic and inorganic species to form new families of hybrid compounds with specific properties. The principle of the sol gel process is based on a succession of hydrolysis condensation reactions at moderate temperatures [9], to prepare oxides networks.

The process consists of a conversion process of metal alkoxides, such as silicon alkoxides, zirconium, aluminum, titanium … The soluble metal species may also contain organic components which may be adjusted according to specific applications.

To our knowledge, only few works on the synthesis of the crednerite $CuMnO_2$ are reported in the literature. $CuMnO_2$ is usually prepared by solid state reaction [6] or ionic exchange re action [10]. More recently, Toufiq et al. have used hydrothermal synthesis to prepare $Cu_{0.4}5Mn_{0.55}O_2$[11], while Chen et al. have reported $Cu_{1.1}Mn_{0.9}O_2$ thin films onto quartz substrates by spin coating [12]. On the other hand, $CuMnO_2$ is an attractive photo catalyst due to its layered lattice which can intercalate oxygen species [13]. The J T ion Mn^{3+} is photoelectrochemically active since it can generate polarization domains that favor the charge separation [7]. Since the X ray diffraction with temperature has not been reported on powder, the present work is devoted to the preparation of $CuMnO_2$ by sol gel method in an air free atmo sphere along with the structural, optical and photo electro chemical characterizations.

2. Experimental

$CuMnO_2$ was prepared by sol gel route according to the fol lowing protocol: $Cu(NO_3)_2 \cdot 3H_2O$ (> 99%, Merck) was mixed to a solution of $Mn(NO_3)_2 \cdot 6H_2O$ (> 98%, Alpha Aesar) with a molar ratio (0.025/0.025) in ethylene glycol (60 mL, 99% BDH) and

* Corresponding author.
E-mail address: solarchemistry@gmail.com (M. Trari).

http://dx.doi.org/10.1016/j.mssp.2016.07.012

maintained under magnetic agitation (350 rpm) for 2 h. The mixture was heated at 70 °C (6 h) at reflux; and the viscous solution was dried at 120 °C during four days. The gelation occurred on a hot plate till a brown color appeared. Then, the amorphous powder was heated at 450 °C in air (2.5 °C/min) for the total denitrification and elimination of organic residues. Thermo gravimetric analysis (TGA) of the powder (20 mg) was performed up to 900 °C (2.5 °C/min) under nitrogen flow (99.9995%) using a Setaram TAG 1750 apparatus to follow the course of the reaction. The powder was calcined at 900 °C in an alumina crucible (8 h) under nitrogen flow. The end product exhibits a black brown coloration. The X ray diffraction (XRD) was recorded in the 2θ range (15 100°) using X ray diffractometer (Bruker D4 Endeavor) with Cu Kα radiation (λ=0.154178 nm) up to 900 °C, the patterns were compared with the JCPDS cards using Eva Program. The particle size was determined from a particle size analyzer (Mastesizer 3000, Malvern Instruments); $CuMnO_2$ powder was suspended in distilled water using an ultrasonic bath for 15 min. The surface morphology was examined with a scanning electron microscope (SEM, Microscope Jeol 6510LV) operating at 20 kV.

$CuMnO_2$ was dissolved in acid and the chemical analysis was carried out by inductively coupled plasma (ICP, Varian Vista Pro CCD, and Simultaneous ICP OES). The concentration was determined by interpolation from a calibration plot. The FTIR spectrum was recorded with a Nicolet spectrometer 6700; the powder (~15%) was pressed into disks using dried spectroscopic KBr. The Raman spectrum was measured on the $CuMnO_2$ powder over the range (300 1200 nm) using a Jobin Yvon T64000 spectrometer; 514.5 nm lines Ar^+ laser excitation was provided from a Spectra Physics Krypton ion laser (4 W) and the beam was concentrated on the sample. The diffuse reflectance was measured with a double beam spectrophotometer (Specord 200 Plus). The powder was pressed into pellets (⌀=13 mm) under a pressure of 200 MPa and fired at 1000 °C under N_2 blanket. The dimensions and weight of the pellets were used to evaluate the density of $CuMnO_2$ (73%); conductive silver paint was used for the electric contact. The conductivity was measured by the two probe method under argon atmosphere using an Agilent LCR meter 4363B. The working electrode ($CuMnO_2$, 1.32 cm^2) was encapsulated in a glass holder with epoxy resin. A conventional cell with Pt electrode (Tacussel) and a saturated calomel electrode (SCE), were used for the plot of the intensity potential J(V) curves. The working electrode was illuminated with a tungsten lamp (200 W, Phillips) through an optical window, positioned below the cell. The potential was controlled with a PGZ 301 potentiostat (Radiometer analytical) with a scan rate of 10 mV s^{-1}. The electrolytic KOH solution (0.5 M) prepared in distilled water was continuously bubbled with pure nitrogen and all tests were carried out at ambient temperature.

3. Results and discussion

Heating the powder at 450 °C in air permits the elimination of water, nitrates and ethylene glycol. The XRD analysis is illustrated in Fig. 1, the spectrum shows only the peaks of the tenorite CuO (JCPDS card No 48.1548), bixbyite Mn_2O_3 (JCPDS card No 41.1442) and spinel $Cu_xMn_{3-x}O_4$ (JCPDS card No 074.1921). The TG plot of the powder heated under N_2 atmosphere (Fig. 3a) shows a weight loss at ~200 °C ascribed to water vaporization, while the loss in the range (700 750 °C) is due to the reduction of CuO to Cu_2O, according to the stability diagram of CuO where the transition CuO/Cu_2O occurs at 723 °C [14], this value is close to the reduction temperature of our TGA curve, which requires a residual pressure of 1.68×10^{-4} atm for CuO. In this work, under very high N_2 flow, one can estimate $p(O_2)$ less than that in nitrogen bottle (with P

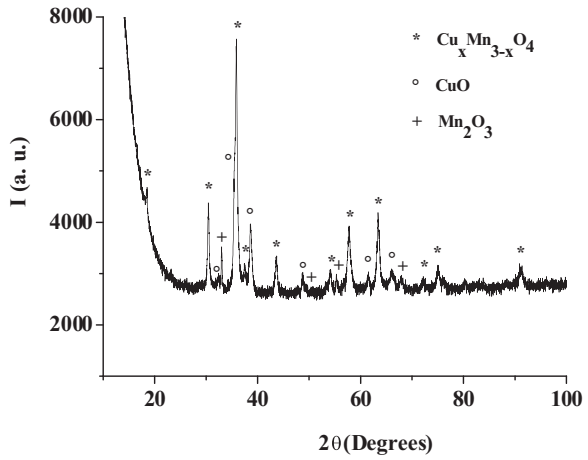

Fig. 1. XRD pattern of powder heated after heating to 450 °C in air.

$(O_2)=10^{-6}$ atm). Indeed, Chen et al. [12] have deposited films of $Cu_{1.1}Mn_{0.9}O_2$ onto quartz substrate using sol gel processing, they first treated the powder at 500 °C in air to stabilize the oxidation states Cu^{2+} and Mn^{3+}, $Cu_xMn_{3-x}O_4$ and CuO were obtained. Then, they annealed the mixture in the temperature range (600 750 °C) in N_2 atmosphere. $CuMnO_2$ was formed above 600 °C, indicating a reduction of Cu^{2+} to Cu^+. Besides that, Kurokawa et al. [15] have investigated a two step process both in air and under argon flow. They found that the sample annealed at 350 °C in air leads to the formation of $CuMn_2O_4$ while the calcination in argon atmosphere between 750 and 950 °C leads to pure crednerite $CuMnO_2$. So, we can deduce that the transition $2CuO \rightarrow Cu_2O + \frac{1}{2}O_2$ starts at ~600 °C under inert atmosphere. Following our XRD results at 450 °C in air (Fig. 1), the spinel $Cu_xMn_{3-x}O_4$ and single oxides CuO and Mn_2O_3 are present with molar percentages of 42.7, 43.1 and 14.5 respectively according to the structural refinement. Hence, we can propose two different mechanisms for the formation of $CuMnO_2$:

a) One step

$$\frac{1}{(3-x)}Cu_xMn_{3-x}O_4 + \frac{(3-2x)}{3-x}CuO \rightarrow \frac{1}{2(3-x)}O_2 + CuMnO_2(x=1) \quad (1)$$

b) Two step

$$2CuO \rightarrow Cu_2O + \frac{1}{2}O_2 \quad (2)$$

$$Mn_2O_3 + Cu_2O \rightarrow 2CuMnO_2 \quad (3)$$

The two equations give the final reaction:

$$2CuO + Mn_2O_3 \rightarrow 2CuMnO_2 + \frac{1}{2}O_2 \quad (4)$$

On the other hand, Götzendörfer [16] reported that a thermal treatment of dip coated copper manganese oxide in air in the temperature range (400 700 °C) stabilizes the cubic spinel $Cu_xMn_{3-x}O_4$, which contain Cu^{2+} ions and mixed valences of manganese (Mn^{3+}/Mn^{4+}). So, high temperatures favor small x values (< 1.5) i.e low Mn (IV) content as evidenced by the existence of a small amount of CuO. Such result is also consistent with the XRD quantification which indicates x value of 1.33 for a molar ratio Cu/Mn=1. Ping et al. have shown that both the temperature and cation ratio have a strong effect on the stoichiometry of $Cu_xMn_{3-x}O_4$ [5].

It is worthwhile to mention that at 450 °C in air, the pattern (Fig. 2) shows only the peaks of CuO, Mn_2O_3 and $Cu_xMn_{3-x}O_4$.

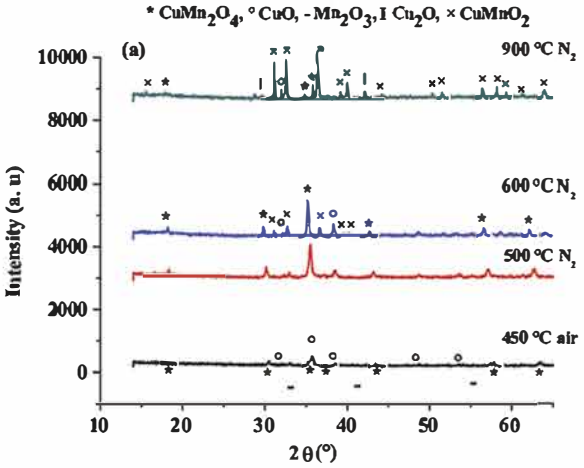

Fig. 2. Sol-gel copper manganese oxide annealed in air at 450 °C and post annealed under N_2 flow. The structural evolution is shown as function of temperature.

However, the peaks of the spinel decrease in intensity above 600 °C under N_2 flow while the characteristic peaks of the cred nerite start to appear (2θ = 15.49°, 36.77°, 39.61°, 40.21°, 47, 13°).

The XRD analysis recorded after calcination at 900 °C under nitrogen flow shows the formation of the crednerite $CuMnO_2$ (Fig. 3b) in agreement with the literature data [6,17,18]. The XRD pattern, free from secondary phases, is indexed in a monoclinic unit cell with the space group *C*2/*m* according to the JCPDS card No 01.083.0034. The lattices parameters of $CuMnO_2$ refined in the *C*2/*m* space group by the Rietveld method are: a = 5.59585 Å; b = 2.8826(2) Å; c = 5.89075 Å and β = 104° (Fig. 3b). The phase $CuMnO_2$ synthetized by sol gel method as a particle size dis tribution in the range 200 400 nm determined from granulometry as shown in Fig. 4a and confirmed by XRD with the intercept at θ = 0 for the Williamson Hall in Fig. 4b plot being (71 ± 6 nm).

The atomic coordinates (x0z) of oxygen (position *4i* of the space

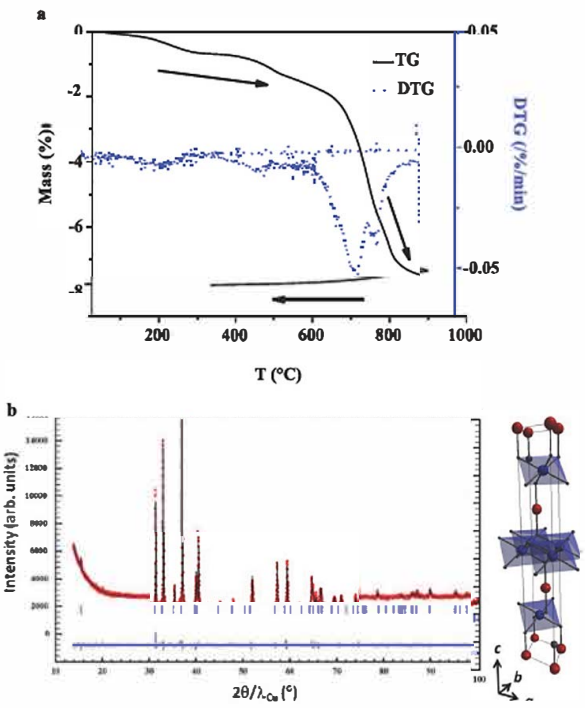

Fig. 3. (a) TGA and DTG plot under high purity N_2 (5 °C/min), of the powder prepared by heat treatment at 450 °C (1 h). (b) Rietveld refinement and structure of the crednerite $CuMnO_2$ synthesized by sol-gel method and annealed at 900 °C under N_2 flow.

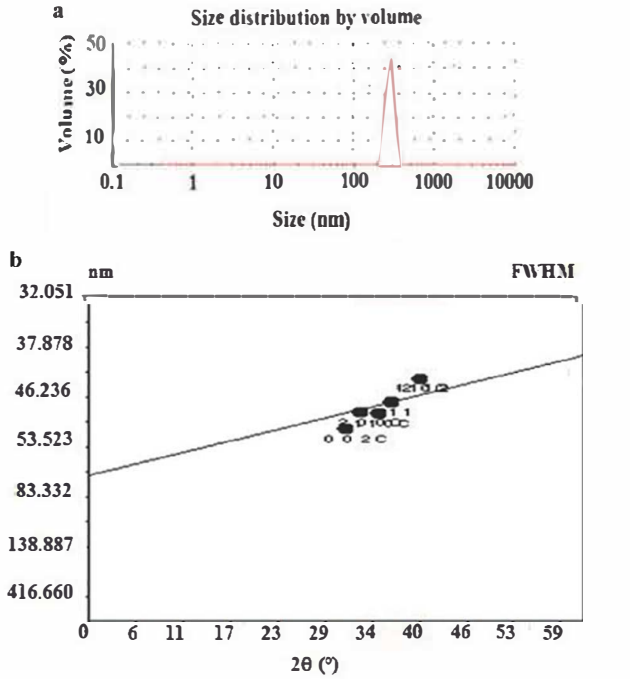

Fig. 4. Grain/particle size analysis of powdered $CuMnO_2$: (a) Particle size distribution from granulometry (by volume). (b) A Williamson-Hall plot showing the average particle size from the intercept. The particle size is found to be 71.03 ± 5.49 nm (correlation coefficient 0.893).

group, unit axis b, cell choice 1) are x = 0.404(1) and z = 0.175(2). Mn^{3+} and Cu^{+} ions are located in particular positions 2*a* (0 0 0) and 2*d* (0 1/2 1/2) respectively. The pattern can be fitted with all recorded peaks and an excellent matching between the observed and fitted intensities is obtained.

The layers of MnO_6 octahedra joined by common edges are linked to each other by monovalent Cu^{+} forming linear link O Cu O (Fig. 5). The manganese form triangular sublattices stacked along the [001] direction in a three sheet repeat units ABCABC. The MnO_6 octahedron is elongated along the [001] direction, leading to an orbital ordering of occupied d_{z^2}. The $d_{x^2-y^2}$ orbital are directed toward the four closer oxygen atoms in the (a, b) planes, while the d_{z^2} orbital with odd number of electron gives rise to an antiferromagnetism with a Neel temperature of 42 K [19]. Ac cordingly, a monoclinic symmetry is obtained because of the lift of degeneracy of Mn^{3+} ion where the Mn O distances (Table 1) differ from those calculated from the sum of ionic radii (d(Mn^{3+}_{VI-HS} O^{2-}_{IV} = 2.025 Å)) [20]; the large *c*/*a* value is ascribed to Mn^{3+} ion in high spin (HS) configuration (t_{2g}^3 $d_{z^2}^1$ $d_{x^2-y^2}$°). The distortion of MnO_6 octahedron, agrees with two long apical Mn O bonds at 2.260 Å and four short in the plan (a, b) at 1.929 Å, leading to an elongation of the MnO_6 octahedron (Mn $O_{//}$/Mn $O_{\perp}$ = 1.17). The length Cu O (1.86 Å) is in perfect agreement with that calculated from the sum of ionic radii of $^{II}Cu^{+}$ (0.46 Å) and $^{IV}O^{2}$ (1.38 Å) [20], thus confirming the ionicity and linearity of the [O Cu O]$^{3-}$ unit. The Cu O Cu bond adjoining two MnO_6 octahedra belonging to successive layers is slightly bent below the ideal value of 180°. Selected interatomic distances are reported in Table 1.

The thermal stability of $CuMnO_2$ was also investigated and the thermal analysis was plotted in air (Fig. 5a). The weight increases progressively and reaches a maximum at 560 °C, accounting for 6.53%; it corresponds to the spinel $Cu_xMn_{3-x}O_4$ (x = 1.37) and is close to that reported by Ping et al. [21]. The weight loss at ~1000 °C corresponds to the reformation of the crednerite; such results agree with those of Bessekhouad et al. [10] and two reac tions can be proposed:

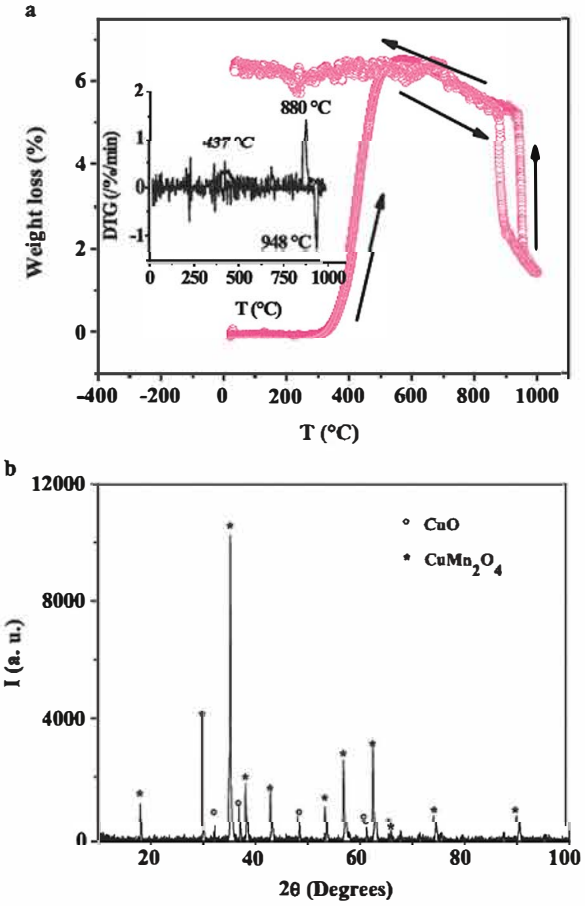

Fig. 5. (a) Analysis of a sample annealed at 1000 °C in air. (a) TGA and DTG (Inset) and (b) XRD pattern indicating a mixture of CuO and $CuMn_2O_4$.

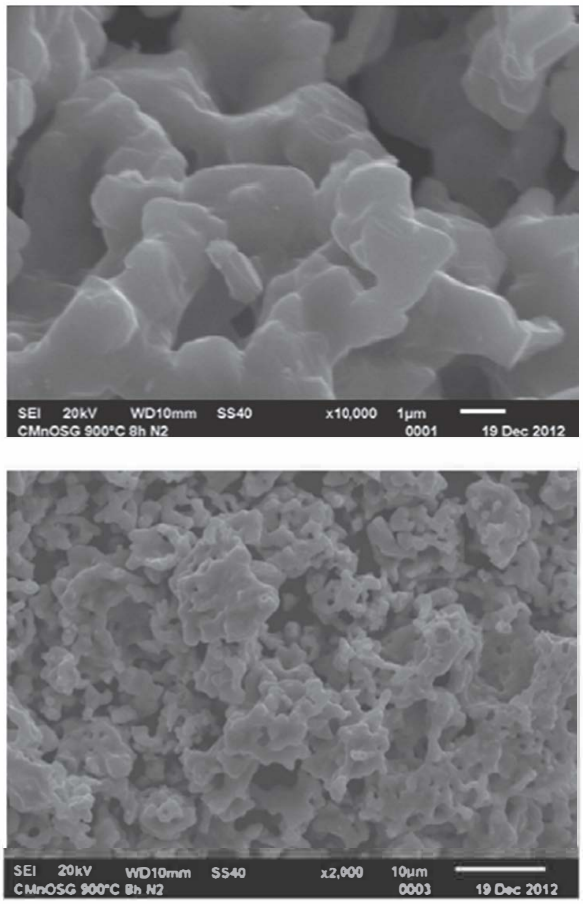

Fig. 6. SEM images at different magnifications of $CuMnO_2$ powder synthesized by sol-gel method and annealed at 900 °C under N_2 flow.

Table 1
Interatomic distances in $CuMnO_2$.

Interatomic distances	(Å)
Mn-O_1	2.28
Mn-O_4	1.92
Cu-O	1.86
O_1-O_2	3.12
O_1-O_4	2.84
O_2-O_3	2.61
O_3-O_4	2.88

$$(3-x)CuMnO_2 + \frac{1}{2}O_2 \rightarrow Cu_xMn_{3-x}O_4 + (3-2x)CuO \quad x=1.37 \tag{5}$$

$$\frac{1}{(3-x)}Cu_xMn_{3-x}O_4 + \frac{(3-2x)}{(3-x)}CuO \rightarrow CuMnO_2 + \frac{1}{2(3-x)}O_2 \quad x=1 \tag{6}$$

The peaks at 437 and 950 °C in the DTG plot (Fig. 5a, Inset) are attributed to the formation of $Cu_{1.37}Mn_{1.63}O_4$ and $CuMnO_2$ respectively. During the cooling, the peak at 880 °C is assigned to the oxidation of $CuMnO_2$ into spinel and tenorite, in agreement with the results reported by some of us [10]. The oxide heated at 1000 °C in air and slowly cooled indicates an oxidation to the cubic spinel (JCPDS Card No 01.071.1143) and CuO (JCPDS Card No 01.080.0076), as evidenced from the XRD analysis (Fig. 5b).

The Cu/Mn ratio of the crednerite $CuMnO_2$, determined by inductively coupled plasma, is found to be equal to unity, a result consistent with the XRD analysis. Mn^{3+} is more oxidant than Cu^+ and the formulation (Cu^+/Mn^{3+}) in the crystal lattice is maintained by the lattice energy. However, in acid solution (pH~2) $CuMnO_2$ is dissolved and the reaction $\{CuMnO_{2(s)} + 4h^+ \rightarrow Cu^+_{(aq)} + Mn^{3+}_{(aq)} + 2H_2O\}$ is shifted to the right side, thus permitting the determination of the average valence of copper by chemical titration [10]; the found value (1.03) is obtained which corresponds to an oxygen excess (δ) of 0.015 in $CuMnO_{2+\delta}$. It is quite logical to find a low value because the radius of Mn^{3+} ($r=0.645$ Å) is smaller than the limit distance for the oxygen incorporation ($r_c=0.70$ Å) in the crednerite lattice. Consequently, the phase transition to the spinel is favored in such a case [22].

The SEM image of $CuMnO_2$ (Fig. 6) shows a uniform morphology with dense particles of similar sizes and shapes; the particle size is 0.5 2 μm. The EDS analysis shows that the final oxide contains Mn, O, and Cu in stoichiometric ratios, suggesting that the synthesized nanostructures are made of pure crednerite $CuMnO_2$. Indeed, the analysis (Table 2) agrees with the nominal composition and shows a homogeneous elemental distribution with a Mn/Cu molar ratio of 1.13 (the percentages are Mn=36.12% and Cu=41.03%, these being very close to the theoretical ones 36.50% and 42.22% respectively).

The crystallographic location of inorganic ions is corroborated

Table 2
EDS obtained data of $CuMnO_2$.

Elements	$W_{théo}$ (%)	W_{exp} (%)	At (%)
Mn	36.50	36.12	24.07
Cu	42.22	41.03	23.64
O	10.62	22.85	52.29

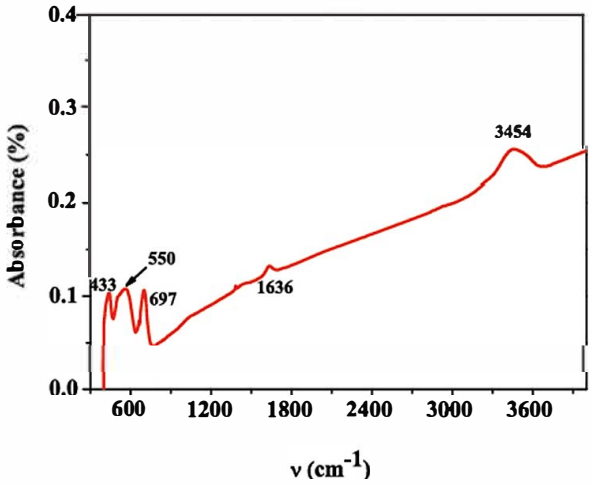

Fig. 7. FTIR spectrum of $CuMnO_2$ synthesized by sol-gel method and annealed at 900 °C under N_2 flow.

by the infrared spectroscopy [23]. The bands in the range (400 1000 cm $^{-1}$) are assigned to active vibrations in mineral oxides. While, the bands at 1630 and 3440 cm $^{-1}$ are due to the bending and stretching modes of adsorbed water (Fig. 7). The spectra of manganese based oxides are divided into three domains (250 450 cm $^{-1}$), (450 600 cm $^{-1}$), and (600 750 cm $^{-1}$), attributed respectively to the vibrations of stretching, bending and wagging in MnO_n polyhedra [24]. The peaks in the range (700 400 cm $^{-1}$) are due to Mn O vibrations in Mn^{3+} based compounds [25] while the peak at 550 cm $^{-1}$ corresponds to the vibration of monovalent copper linearly coordinated by O^{2-} ions [26].

The delafossite structure has two Raman active modes; the mode A_{1g} attributed to O Cu O vibration along the *c* axis and the mode E_g derived from MO_6 octahedra along the *a* axis [27 29]. The active mode A_{1g} is around ~700 cm $^{-1}$ for the delafossites $CuMO_2$ (M=Al, Cr, Fe) [27 29]. Our spectrum (Fig. 8) shows a single intense peak at 679 cm $^{-1}$ attributed to A_{1g} mode [30]; such result is corroborated by Runka et al. which have assigned the peak at 675 cm $^{-1}$ to symmetric stretching vibrational modes of MnO_6 octahedra [31].

The fundamental optical transition in the reflectance diffuse spectrum is used to determine the forbidden band (E_g) using the Tauc relation:

$$(\alpha h\nu)^{1/n} = Cons\tan t \times (h\nu - E_g) \quad (7)$$

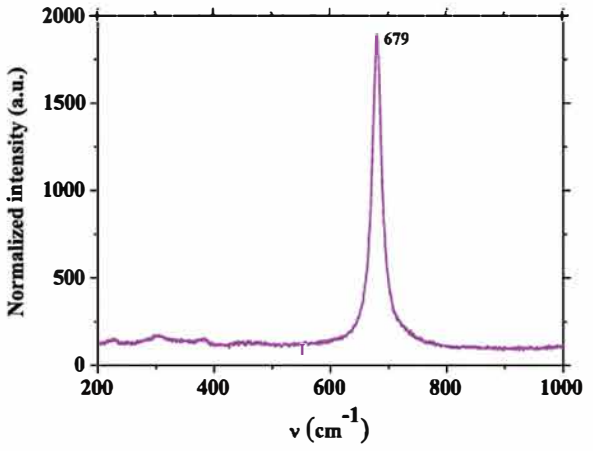

Fig. 8. The Raman spectrum of $CuMnO_2$ synthesized by sol-gel method and annealed at 900 °C under N_2 flow, recorded at room temperature.

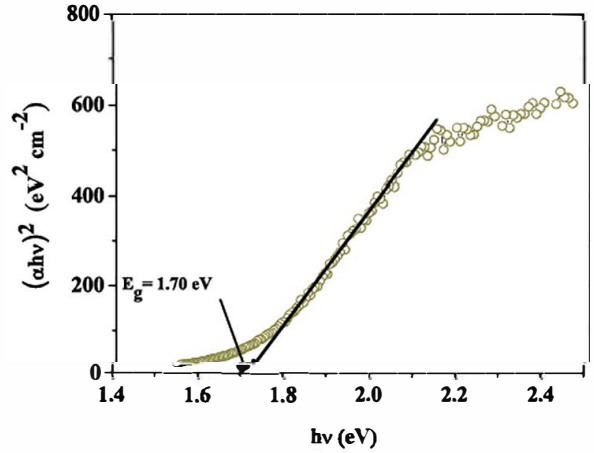

Fig. 9. The direct optical transition of $CuMnO_2$ synthesized by sol-gel method and annealed at 900 °C under N_2 flow.

where α is the optical absorption coefficient and hν the energy of the incident photon. The exponent *n* is equal to 1/2, 2 and 3/2 respectively for direct, indirect and direct forbidden transitions. From the plot of $(\alpha h\nu)^{1/n}$ versus hν (Fig. 9), a direct transition is obtained at 1.70 eV, due to interband transition *d d*, in conformity with the black brown color of $CuMnO_2$, this transition is close to that obtained elsewhere [32].

The transport properties of $CuMO_2$ are strongly dependent on their chemical compositions and particularly on the deviation from stoichiometry. Metal oxides are non stoichiometric because of mixed valences of *3d* elements. The increase of the electrical conductivity (σ) with raising temperature indicates a semiconducting behavior of $CuMnO_2$ (Fig. 10); the thermal variation obeys to an exponential type law with $\sigma_{300\,K}$ value of ~$5 \times 10^{-4}\,\Omega^{-1}\,cm^{-1}$ [10,12]. The data are fitted by the least square method and the activation energy E_a (=0.21 eV) is in conformity with a conduction mechanism by low polarons jump between mixed states Cu^{2+}/Cu^{+} in the (a, b) planes by phonon [2,12]. The electrons move by phonon assisted hopping between nearest sites owing to the electron phonon interaction. Indeed, the inter ionic Cu^{+} Cu^{+} distance, equal to the lattice constant *a*, is large enough to accommodate O^{2-} ions (radius=0.140 nm) in the bi dimensional lattice of $CuMnO_2$. An equivalent amount of Cu^{2+} is formed (=2δ) to maintain the charge neutrality. The oxidation state of copper increases slightly and deviates from unity. Hence, $CuMnO_2$ exhibits *p* type behavior, thus allowing the oxide to be characterized electrochemically.

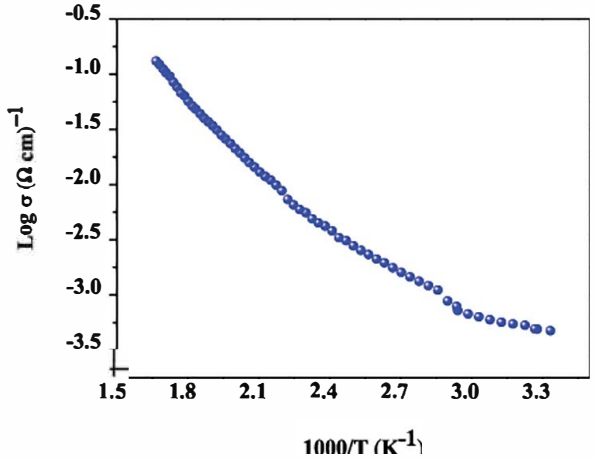

Fig. 10. Variation of log (σ) versus temperature in the crednerite $CuMnO_2$ synthesized by sol-gel and annealed at 900 °C under N_2 flow.

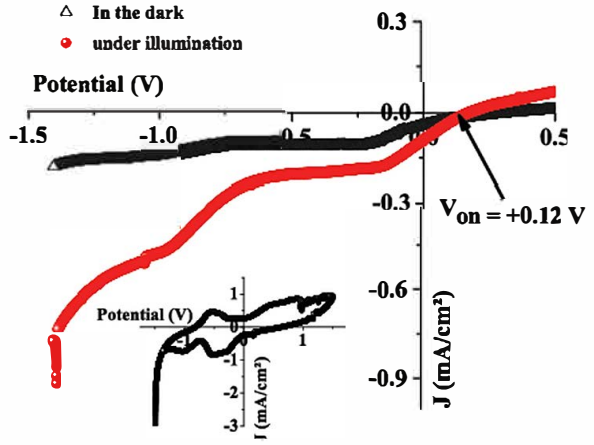

Fig. 11. The variation of the current density (J) versus the potential (V) of $CuMnO_2$ synthesized by sol-gel and annealed at 900 °C under N_2 flow, in the dark and under illumination in KOH solution (0.5 M) at 25 °C, scan rate 10 mV s^{-1}. Inset: the J (V) curve in the dark.

The photo electrochemical characterization of $CuMnO_2$ is rea lized in KOH (0.5 M) where the oxide exhibits an excellent che mical stability (Fig. 11). The intensity potential (J V) curve was scanned from 1.5 V toward positive potentials because of the *p* type conductivity. The dark current (J_d) is smaller than 1 mA cm^{-2}, indicating an electrochemical stability over a large potential range. While, the significant current above 1 V is due to H_2O oxidation. The (J_d V) characteristic in the cathodic side intercepts the ab scissa axis at a potential of the hydrogen evolution reaction (HER) and is function of the partial pressure of oxygen. In aerated solu tion, the potential of the couple H_2O/H_2 (0.75 V) is obtained by prolonging the line to the potential axis. The peak at ~0.44 V (Fig. 11, inset) is due to the electrochemical couple $Cu^{+/2+}$ and is close to the standard redox potential [33], the electro neutrality condition implies oxidation of $CuMnO_2$ according to the electro chemical process:

$$CuMnO_2 + 2\delta OH^- \rightarrow CuMnO_{2+\delta} + \delta H_2O + 2\delta e^- \quad (8)$$

δ stands for the amount of inserted O^{2-} ions in the two di mensional lattice. The electrical charge under the anodic peak, determined by integration of the surface area, averages 5 mC cm^{-2} and corresponds to the oxidation of $\sim 3 \times 10^{16}$ at. Cu^+ cm^{-2}. The peak at ~ 0.33 V, is ascribed to the electrochemical couple Cu^{3+}/Cu^{2+}, and is close to that observed in La_2CuO_4, responsible of the superconductivity at ~40 K [34]. The peak at 0.23 V, upon back scanning, corresponds to oxygen deintercalation but the difference exceeds the value 0.06 V/n which indicates that the oxygen in sertion is irreversible and the shape of the curve (J_{ph} V) and the increase of photocurrent J_{ph} along the negative polarization con firm *p* type behavior with holes as majority charge carriers. J_{ph} starts to appear at a potential of +0.12 V, thus corroborating the previous results [10] and increases gradually to attain a plateau region beyond 0.15 V. Such saturation is mainly due to a ne glected recombination process of (e^-/h^+) pairs. Below 0.3 V, the photocurrent J_{ph} reaches a maximal value which depends only on the light intensity and indicates that all generated (e^-/h^+) pairs contribute to the photocurrent. The detailed electrochemical characterization is currently under progress and will be reported soon.

4. Conclusion

Pure crednerite $CuMnO_2$ was prepared by sol gel processing. A monoclinic structure was obtained at 900 °C under very pure nitrogen flow. The lattice constants were determined from the Rietveld refinement and the SEM images showed that the cred nerite possesses a porous morphology having dense individual grains. The room temperature Raman spectrum showed a single peak assigned to A_{1g} mode in MnO_6 octahedra. The direct optical transition in the visible region is attributed to Cu^+ *d d* transition. The thermal evolution of the electrical conductivity confirmed the semiconducting properties of the crednerite. The photoelec trochemical study showed *p* type behavior due to the oxygen in tercalation in the layered crystal lattice.

Acknowledgments

The authors are grateful to the Ministry of Scientific Research (Algeria) for the research grant and the group of Mixed Valence Oxide at CIRIMAT UMR CNRS (P. Sabatier University, Toulouse III France) for welcoming one of the authors (N. B.).

References

[1] N. Koriche, A. Bouguelia, M. Mohammedi, M. Trari, J. Mater. Sci. 42 (13) (2007) 4778–4784.
[2] B. Bellal, B. Hadjarab, N. Benreguia, Y. Bessekhouad, M. Trari, J. Appl. Electrochem. 41 (2011) 867–872,
[3] D. Kumar, S. Kumar, V.G. Sathe, Solid. State Commun. 194 (2014) 59–64.
[4] R. Yang, F. Chen, RSC Adv. 5 (2015) 974–980.
[5] P. Wei, M. Bieringer, L.M.D. Cranswick, A. Petric, J. Mater. Sci. 45 (2010) 1056–1064.
[6] M. Trari, J. Töpfer, P. Dordor, J.C. Grenier, M. Pouchard, J.P. Doumerc, J. Solid. State Chem. 178 (2005) 2751–2758.
[7] Y. Bessekhouad, M. Trari, J.P. Doumerc, Int. J. Hydrog. Energy 28 (2003) 43–48.
[8] G. Fierro, G. Ferraris, R. Dragone, L.L. Jacono, M. Faticanti, Catal. Today 116 (2006) 38–49.
[9] A.C. Pierre, G.M. Pajonk, Chem. Rev. 102 (2002) 4243–4265.
[10] Y. Bessekhouad, Y. Gabès, A. Bouguelia, M. Trari, J. Mater. Sci. 42 (2007) 6469–6476.
[11] A.M. Toufiq, F. Wang, Javed Qurat-ul-ain, Q. Li, Y. Li, Mater. Lett. 118 (2014) 34–38.
[12] H.Y. Chen, D.J. Hsu, Appl. Surf. Sci. 290 (2014) 161–166.
[13] W. Ketir, A. Bouguelia, M. Trari, J. Hazard. Mater. 158 (2008) 257–263.
[14] J. Neumann, T. Zhong, Y. Chang, Bull. Alloy Phase Diagr. 5 (1984) 136–141.
[15] A. Kurokawa, T. Yanoh, S. Yano, Y. Ichiyanagi, J. Nanosci. Nanotechnol. 14 (2014) 2553–2556 (4).
[16] S. Götzendörfer, PhD Thesis, Wurzburg, 2010.
[17] Lu.D. Kondrashev, Sov. Phys.: Cristallogr. 3 (1959) 703–706.
[18] McAndrew, Am. Mineral. 41 (1956) 276-287.
[19] M. Trari, PhD thesis, Bordeaux, 1994.
[20] R.D. Shannon, Acta Crystallogr. A32 (1976) 751–767.
[21] Y. Ping, Y. Bo, Z. Lei, Sci. China Ser. B-Chem 52 (1) (2009) 101–108.
[22] E. Mugnier, A. Barnabé, P. Tailhades, Solid. State Ion. 177 (5–6) (2006) 607–612.
[23] K. Nakamoto, Infrared and Raman Spectra of Inorganic and Coordination Compounds, Theory and Applications in Inorganic Chemistry Hardcover, John Wiley and Son edition, Inc Hoboken, New Jersey, 2009.
[24] C.M. Julien, M. Massot, C. Poinsignon, Spectrochim. Acta A 60 (2004) 689–700.
[25] B. Gillot, M. El Guendouzi, M. Laardj, Mater. Chem. Phys. 70 (2001) 54–60.
[26] B. Saha, R. Thapa, K.K. Chattopadhyay, Mater. Lett. 6 (2009) 394–396.
[27] O. Aktas, K.D. Truong, T. Otani, G. Balakrishnan, M.J. Clouter, T. Kimura, G. Quirion, J. Phys: Condens. Matter 24 (2012) 036003–036010.
[28] S.P. Pavunny, A. Kumar, R.S. Katiyar, J. Appl. Phys. 107 (2010) 013522-013529.
[29] M.K. Singh, S. Dussan, G.L. Sharma, R.S. Katiyar, J. Appl. Phys. 104 (2008) 113503–113507.
[30] H.Y. Chen, Y.C. Lin, J.S. Lee, Appl. Surf. Sci. 338 (2015) 113–119.
[31] T. Runka, M. Berkowski, J. Mater. Sci. 47 (2012) 5393–5401.
[32] Q. Zhang, D. Xiong, H. Li, D. Xia, Haizheng Tao, Xiujian Zhao, J. Mater. Sci: Mater. Electron. (2015) 1–5, http://dx.doi.org/10.1007/s10854-015-3702-z.
[33] D.R. Lide, Handbook of Chemistry and Physics, 78th ed., McGraw-Hill, New York, 1997.
[34] J.C. Grenier, A. Wattiaux, N. Lagueyte, J.C. Park, E. Marquestaut, J. Etourneau, M. Pouchard, Physica C173 (1991) 139–144.